# Linear versus Exponential Growth of Weak Polyelectrolyte Multilayers: Correlation with Polyelectrolyte Complexes

**ARTICLE** *in* MACROMOLECULES · APRIL 2012

Impact Factor: 5.8 · DOI: 10.1021/ma300157p

Macromolecules

Article

pubs.acs.org/Macromolecules

# Linear versus Exponential Growth of Weak Polyelectrolyte Multilayers: Correlation with Polyelectrolyte Complexes

Li Xu,[†] Denis Pristinski,[‡] Aliaksandr Zhuk,[†] Chris Stoddart,[†] John F. Ankner,[§] and Svetlana A. Sukhishvili*,[†]

[†]Department of Chemistry, Chemical Biology and Biomedical Engineering, Stevens Institute of Technology, Hoboken, New Jersey 07030, United States

[‡]BioSensors Division, NantWorks LLC, Costa Mesa, California 92626, United States

[§]Spallation Neutron Source, Oak Ridge National Laboratory, Oak Ridge, Tennessee 37831, United States

Supporting Information

**ABSTRACT:** We report on the correlation of polyelectrolyte chain dynamics in polyelectrolyte complexes (PECs) with the deposition mode and chain mobility of polyelectrolytes (PEs) within layer-by-layer-assembled (LbL) films. The study was performed using two polyelectrolyte systems: poly(2-(dimethylamino)ethyl methacrylate)/poly(methacrylic acid) (PDMA/PMAA) and completely quaternized PDMA (Q100M)/PMAA. Hydrodynamic sizes of PDMA/PMAA and Q100M/PMAA complexes in solution were followed by fluorescence correlation spectroscopy (FCS), while three different techniques were applied to probe the structure and dynamics of the same PE pairs within LbL films. Specifically, deposition of PEs at surfaces was monitored by phase-modulated ellipsometry, film internal structure—by neutron reflectometry (NR), and diffusion of assembled chains in the direction parallel to the substrate—by fluorescence recovery after photobleaching (FRAP). By applying these complementary techniques to PDMA/PMAA and Q100M/PMAA systems in solution and at surfaces at various pH values, we found that the dynamics of polyelectrolyte chains within PECs underwent a prominent pH-dependent transition, and that this transition in chain dynamics was closely correlated with the transition between linear and exponential film growth modes. Neutron reflectometry results confirm that, at the transition point, film structure changed from layered for linearly depositing films to highly intermixed for exponentially depositing LbLs. Moreover, FRAP indicated a several-fold difference in PE lateral diffusion coefficient for the two different film growth modes. In addition, the pH transition point was affected by steric restrictions to ionic pairing, and the pH range of exponential growth and higher chain mobility was wider for Q100M/PMAA as compared with the PDMA/PMAA system, due to the presence of a methyl spacer at the amino group, resulting in weaker ionic pairing.

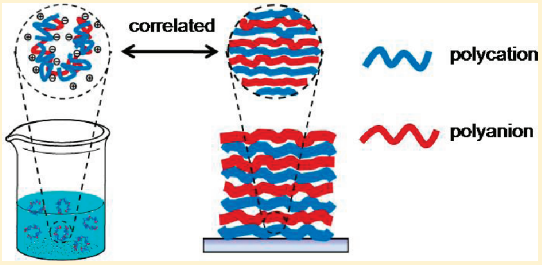


## INTRODUCTION

Since its introduction in the early 1990s,[1] layer-by-layer (LbL) assembly of polymer films has become increasingly widely used for modification of surfaces and preparation of free-standing films. Among many often discussed advantages of the technique, such as the capability to create conformal coatings and its applicability to a wide range of synthetic and biological macromolecules,[2−4] nanoscopic layering in these films is viewed as a unique and desirable feature.[5,6] Yet, it has long been known that the regular layering of polymers within polyelectrolyte multilayers (PEMs) is not a universal phenomenon. Specifically, nonlinear deposition of polymer mass as a function of layer number has been observed with pairs of relatively weakly bound natural polyelectrolytes (PEs).[7−10] This exponential mode of LbL film growth has been directly related to exchange of hydrophilic natural PEs between film and solution during multilayer assembly.[11] Subsequent work resulted in the development of a model which considers the roles of the Donnan potential, the entropic contribution of counterions, and the buildup of an electrostatic barrier for chain diffusion in a dynamic film assembly process.[12] With time, greater experimental evidence accumulated that the exponential growth mode of LbL films is rather regularly observed in many systems. While one can look at the underlying chain diffusion in exponentially growing multilayers as a factor that prevents a desired film layering, this chain diffusion can, for example, also be used to promote ordering of virus particles at the film surface.[13] Moreover, the fact that exponentially growing films can accept a large amount of polymer, up to hundreds of nanometers per deposition cycle,[14] significantly facilitates preparation of mm-thick films.[15]

Several factors have been reported to favor linear vs exponential deposition of specific polyelectrolyte pairs during PEM deposition. For example, for a given PE pair, a transition

Received: January 19, 2012
Revised: March 22, 2012
Published: April 22, 2012

  

from exponential to linear film growth has been observed with increased number of layers.[16] In later theoretical work, this transition was predicted to be set kinetically, and to occur when the dipping time becomes shorter than the time required for mobile PE chains to distribute uniformly within the film.[17] In another interesting report, Laugel et al. demonstrated that linear film growth is related to strongly exothermic PE interactions, while exponential growth occurs with weakly exothermic or endothermic PE pairs.[18] Overall, the literature seems to agree that whether the system will be growing linearly or exponentially depends on the strength of PE intermolecular interactions. For example, we have recently demonstrated that LbL films of temperature-responsive triblock copolymers grow exponentially with poly(acrylic acid) , while the growth becomes linear with the stronger binding polystyrenesulfonate.[19] However, it has also become clear that different growth modes cannot be simply assigned to specific chemical systems.[15] Instead, the same PE pairs can grow either linearly or exponentially depending on deposition conditions, which modulate the strength of interpolyelectrolyte interactions, such as salt type and concentration,[20−22] temperature,[23] or solution pH[24−26] in the case of weak PEs.

The relationship between the interactions of PE chains in solution and at surfaces has been established by several groups.[27−29] For example, phase diagrams for aqueous mixtures of two oppositely charged PEs were shown to closely correlate with the deposition of PE chains within LbL films.[29] Nevertheless, studies of such correlations are still rare. The work described here specifically concerns weak PEs (wPEs), whose charge density is controlled by the solution pH. For interactions of wPEs in solution, recent theoretical work by Biesheuvel et al.[30,31] has predicted that an increase in PE ionization results in an increase in the electrostatic energy of interpolyelectrolyte binding and enhanced polyelectrolyte complex (PEC) coacervation. Experiments by Spruijt et al. and Tirrell and co-workers support these theoretical results.[32,33] However, the effect of solution pH on interactions of PE chains in solution has not been studied in the context of deposition of these chains within LbL films.

Here, we present a side-by-side comparison of pH-dependent interactions of PE chains in solution and deposition of PE chains within PEMs. By applying fluorescence correlation spectroscopy (FCS), we study the dynamics of PE pairs in solution, and find that reluctant exchange and heterogeneities in PECs directly correlate with linear deposition of chains at surfaces. Correspondingly, fast chain equilibration within PECs was predictive of exponential film growth. In addition, in agreement with our recent study,[34] we find that the transition between these two regimes in the pH scale is controlled by steric bulk in PE ionic pairing.

## EXPERIMENTAL SECTION

**Materials.** 2-(Dimethylamino)ethyl methacrylate (DMA), *N*-(3-aminopropyl) methacrylamide (APMA), and tetrabutyl methacrylate (*t*BMA) were purchased from Sigma-Aldrich. Poly(methacrylic acid) (PMAA) with $M_w$ = 110 000 g mol$^{-1}$ and a polydispersity index (PDI) of 1.02, as well as branched polyethylenimine (BPEI) with $M_w$ = 25,000 g mol$^{-1}$ and PDI = 2.50 were purchased from Aldrich. Deuterated PMAA (dPMAA) with $M_w$ = 180 000 g mol$^{-1}$ and PDI = 1.10 was purchased from Polymer Source, Inc. All other chemicals were purchased from Aldrich and used without further purification. Alexa Fluor 488 dihydrazide and Alexa Fluor 488 carboxylic acid, succinimidyl ester were purchased from Invitrogen Co., California. Ultrapure Milli-Q water (Millipore) with a resistivity of ∼18 MΩ/cm was used in all experiments.

For ellipsometry experiments, films were deposited on silicon wafers with ⟨100⟩ orientation purchased from Cemat Silicon S.A., Poland. For fluorescence recovery after photobleaching (FRAP) experiments, homemade glass cells were prepared using the procedure described in our earlier publication.[35] For neutron reflectometry (NR) experiments, silicon wafers of 4 in. diameter with one side polished were purchased from the Institute of Electronic Materials Technology, Poland. In attenuated total reflection-Fourier transform infrared (ATR-FTIR) studies, we used a rectangular trapezoidal silicon crystal with dimensions 50 mm × 20 mm × 2 mm purchased from Harrick Scientific.

**Synthesis and Characterization of PDMA Homopolymer and Copolymers.** PDMA homopolymer and a copolymer of DMA with 5 wt % of APMA or *t*BMA were synthesized by atom transfer radical polymerization (ATRP) which has been described elsewhere.[36] For synthesis of PDMA homopolymer, DMA (8.0 mL, 47 mmol), CuBr (33 mg, 0.23 mmol), 1,1,4,7,10,10-hexamethyltriethylenetetramine (HMTETA) (62 μL, 0.92 mmol) and 2-propanol (8.0 mL) were mixed into a 50 mL Schlenk flask. For synthesis of copolymers, 5 wt % of APMA or *t*BMA (of the weight of DMA) was also mixed into the solution. The solution was processed by three freeze−pump−thaw cycles, and then ethyl-2-bromoisobutyrate (34 μL, 0.23 mmol) was injected into the reaction solution under a protection of argon flow. The polymerization was allowed to proceed under continuous stirring under the argon atmosphere for 12 h. The reaction was terminated with liquid nitrogen and the solution was diluted with tetrahydrofuran (THF). The catalyst complex was removed from the solution by passing through a basic aluminum oxide column. After evaporation of THF solvent, the obtained polymers were precipitated by cold hexane and dried in a vacuum oven at 30 °C overnight. The weight-average molecular weights ($M_w$) of PDMA homopolymer and poly(DMA-*co*-APMA) or poly(DMA-*co*-*t*BMA) copolymers were determined to be ∼30 kDa as measured by a combination of gel permeation chromatography (GPC) and $^1$H NMR. The GPC studies performed in THF demonstrated the PDI of PDMA was 1.10.

**Quaternization of PDMA.** Quaternization of PDMA homopolymer to obtain 100% quaternized PDMA (Q100M) was carried out at room temperature.[37] PDMA homopolymer was dissolved in a mixture of methanol/benzene (v:v = 3:1), and a stoichiometric amount of dimethyl sulfate was added to the solution. The mixture was stirred at room temperature overnight. The product was precipitated with ethanol/THF (v: v = 1: 1) three times, and washed with acetone several times. The extent of quaternization was analyzed by $^1$H NMR in $D_2O$ at pH 9 (Figure S1 in the Supporting Information). After quaternization with dimethyl sulfate, a new peak at 3.3−3.4 ppm appeared, reflecting successful quaternization of the dimethylamino proton with a methyl group. The absence of a peak C at δ 2.3−2.5 ppm and a peak at δ 4.2−4.4 ppm corresponding to dimethylamino protons in PDMA indicates complete quaternization of PDMA homopolymer.

**Preparation of Alexa Fluor 488-Labeled PEs.** Labeling of PMAA with Alexa Fluor 488 (Alexa 488) to obtain fluorescently labeled PMAA (PMAA*) was performed in 0.1 M phosphate buffer at pH 5.[38] 10 μL ($6.3 \times 10^{-4}$ mmol) of PMAA solution was mixed with 1 mg ($5.3 \times 10^{-2}$ mmol) of 1-ethyl-3-(3-(dimethylamino)propyl)-carbodiimide hydrochloride and 1.2 mg ($5.3 \times 10^{-2}$ mmol) of *N*-hydroxysulfosuccinimide sodium salt in 0.1 M phosphate buffer at pH 5, and continuously stirred for 1 h. The incubation step was followed by an addition of 30 μL ($18.9 \times 10^{-4}$ mmol) of Alexa Fluor 488 dihydrazide in 0.1 M phosphate buffer at pH 5. The reaction solution was stirred overnight. The solution was then diluted to 3 mL with 0.1 M phosphate buffer solution at pH 7 and dialyzed against 0.01 M phosphate buffer at pH 7 with 0.1 M NaCl for 48 h, and then against Milli-Q water for 24 h. The molecular weight cutoff of the dialysis tubing was 10,000. The dialysis was stopped when no fluorescence could be detected in the outer dialysis water (measured by fluorometry at excitation wavelength 488 nm).

Synthesis and labeling of PDMA to obtain PDMA* were performed using a procedure described elsewhere.[38,39] 0.1 mg poly(DMA-*co*-APMA) copolymer with 5 wt % APMA units was dissolved in 0.1 mL of 0.1 M sodium bicarbonate buffer at pH 9, and the solution was continuously stirred for 30 min. First, 0.5 mg of Alexa Fluor 488 carboxylic acid, succinimidyl ester was dissolved in 0.05 mL of dimethyl sulfoxide, and then slowly added into the copolymer solution while stirring. The reaction was incubated for 2 h at room temperature with continuous stirring. The solution was then diluted to 3 mL with 0.1 M phosphate buffer solution at pH 4. The solution was dialyzed against 0.01 M phosphate buffer with additional 0.1 M NaCl for at least 48 h, and then against Milli-Q water for 24 h using dialysis tubing with a molecular weight cutoff of 3,500. Dialysis was completed when no fluorescence could be detected in the outer dialysis water.

Fluorescently labeled, completely quaternized polycation (Q100M*) was obtained from poly(DMA-*co*-*t*BMA) with 5% of *t*BMA units. First, DMA units of poly(DMA-*co*-*t*BMA) were completely quaternized with dimethyl sulfate using the procedure described above for quaternization of PDMA homopolymer. Then, cleavage of the *t*BMA groups was achieved by treating the quaternized copolymer with trifluoroacetic acid (TFA) (w:w = 10:1) overnight at room temperature. The procedure resulted in poly(DMA-*co*-methacrylic acid (MAA)) copolymer (with 5% of MAA units) which was then labeled with Alexa Fluor 488 using the procedure used for labeling PMAA.

The efficiencies of fluorescent labeling were estimated by comparing the fluorescent intensities of fluorescent labeled polyanion (PA*) and labeled polycations (PC*s), with those of polymer-free Alexa Fluor 488 hydrazide standard solutions ($\lambda_{max}$ = 493 nm, extinction coefficient =68,000 $cm^{-1}$ $M^{-1}$). PMAA* contained approximately one label per 300 monomer units, while PCs* were labeled with one fluorescent tag per 200 monomer units. All solutions were prepared at least 1 h before measurement to allow polyelectrolyte chains to reach equilibrium in solution.

**Fluorescence Correlation Spectroscopy.** FCS measurements were performed with a custom-made setup using a 488 nm excitation provided by a Spectra-Physics Stabilite 2017 laser.[38] The autocorrelation function (ACF), $G(\tau)$, of fluorescent intensity $I(t)$, can be written as[40−42]

$$G(\tau) = \langle \delta I(t) \delta I(t+\tau) \rangle / \langle I(t) \rangle^2 \quad (1)$$

where the temporal fluctuations of fluorescent intensity, $\delta I(t) = I(t) - \langle I(t) \rangle$ were acquired with a PerkinElmer SPCM-AQR photon counter, processed with a Corrvus AFX-125 correlator, and fit with the correlator modeling software. For freely diffusing molecules in solution, $G(\tau)$ is[43]

$$G(\tau) = \frac{1}{N}\left(1 + \frac{4D\tau}{\omega_{xy}^2}\right)^{-1}\left(1 + \frac{4D\tau}{\omega_z^2}\right)^{-1/2} \quad (2)$$

where $D$ is the translational diffusion coefficient of the particles, $N$ is the average number of fluorescent species in the detection volume, and $\omega_{xy}$ and $\omega_z$ are the radii of the detection volume in the $xy$-plane and $z$-direction, respectively. Values of $\omega_{xy}$ and $\omega_z$ in eq 2 were determined from measurements of the diffusion of Rhodamine-110 in 10 nM aqueous solution. From the known diffusion coefficient of Rhodamine-110 of 390 $\mu m^2/s$, the parameters of the excitation volume were determined as $\omega_{xy}$ = 0.205 $\mu$m and $\omega_z$ = 2 $\mu$m. Diffusion of polydisperse samples was analyzed assuming a log-normal distribution of hydrodynamic radii from which the mean size and the distribution standard deviation were deduced.

Measurements were done with solutions contained within home-made glass cells which were prepared using the procedure described in our earlier publication.[35] In a typical experiment, 200 $\mu$L PMAA* solutions at a concentration of $10^{-4}$ mg/mL in 0.01 M phosphate buffer were prepared in the glass cell. Unless otherwise stated, for experiments with PECs, a 10-fold excess of polycation (PC) with respect to polyanion (PA) (i.e., 20 $\mu$L $10^{-2}$ mg/mL PC solution) was added. The hydrodynamic radius, $R_H$, of diffusing species was calculated from the diffusion coefficient $D$ by the Stokes−Einstein equation. The temperature of all measurements was controlled at 25 °C.

**Multilayer Buildup.** PCs and PMAA were dissolved in 0.01 M phosphate buffer solution. Concentrations of all solutions were controlled at 0.2 mg/mL. The silicon wafers were cleaned as described elsewhere.[44] PEM buildup was started with the deposition of BPEI from solution at pH 9 for 15 min, followed by assembly of PCs with PMAA. All solutions were controlled at pH 4.5, 5.5 or 6, and maintained at room temperature. PEMs were fabricated by dipping the silicon substrates in PMAA solution for 15 min, followed by rinsing twice with 0.01 M phosphate buffer solution for 2 min. The PMAA-assembled substrates were then dipped in PC solutions for 15 min and again rinsed with phosphate buffer solution for 2 min. This process was repeated until the desired number of layers had been deposited. The deposition was completed with a layer of PMAA.

**Ellipsometry.** Measurements of dry multilayer thicknesses were performed using a custom-built, single-wavelength, phase-modulated ellipsometer at 65° angle of incidence. For dry films, the refractive indices for the $SiO_2$ layer and dry multilayer films were set at 1.456 and 1.500, respectively. The dry thicknesses of all films were measured after being blown dry in nitrogen flow.

**Neutron Reflectometry.** 24-bilayer films of BPEI/PMAA/$[(PC/PMAA)_4/(PC/dPMAA)]_4$ /$(PC/PMAA)_4$ were prepared for the NR measurements, with dPMAA deposited in every fifth bilayer to provide the neutron scattering contrast. The samples were blown dry with nitrogen, kept in ambient conditions for 1 week, and measured in Oak Ridge National Lab (ORNL).

The neutron reflectivity data was collected at the Spallation Neutron Source Liquids Reflectometer (SNS-LR) at ORNL. A continuous wavelength band $\lambda$ was controlled in the range of 2.5−6.0 Å, and the measurements were performed at seven incident angles of $\theta$ = 0.15, 0.25, 0.45, 0.65, 0.85, 1.60, and 2.80°. The momentum transfer $Q$, defined as $Q = (4\pi(\sin\theta)/\lambda)$, thus spanned a range of 0.006 $Å^{-1}$ < $Q$ < 0.307 $Å^{-1}$. The data sets collected at the seven different angles were combined together to obtain a reflectivity curve. The resolution of instrument was maintained at $\delta Q/Q$ = 0.02 for all measuring angles.

The NR curves were analyzed by a model described earlier.[44] The fitting parameters are listed in Table S1 in the Supporting Information. The neutron scattering density profile was defined by modeling the film structure as adjacent layers with a defined thickness $d$ and scattering density $\Sigma$, as well as an rms interfacial mixing $\sigma$ between adjacent layers. As in our earlier work,[44] it was found necessary to employ models in which the thickness of dPMAA marker layers exceeded the nominal total thickness of densely packed dPMAA, indicating that the original deuterated layers were mixed with the surrounding protonated matrix. The mass deposited within the dPMAA layers was accounted for to preserve mass balance. Because of insignificant contrast between $\Sigma$ values of the hydrogenated polymers, thickness-weighted-average scattering density $\Sigma_p$, thickness $d_p$, and rms roughness $\sigma_p$ were introduced for the protonated PMAA/PC stacks.

**Attenuated Total Reflection Fourier Transform Infrared Spectroscopy (ATR-FTIR).** The growth of the PEMs was monitored *in situ* by a Bruker Equinox-55 Fourier transform infrared spectrometer with attenuated total reflection. LbL films were deposited on a rectangular trapezoidal 50 mm ×20 mm ×2 mm silicon crystal (Harrick Scientific) with 45° beam entrance and exit surfaces. To provide the desired spectroscopic window to follow vibrational bands of the PEM components, films were deposited from $D_2O$ rather than $H_2O$ solutions.[45] $D_2O$ was also used for rinsing during sequential deposition of PEM films. Infrared spectra were collected by the spectrometer with a narrow-band mercury cadmium telluride detector. ATR optics and a temperature-controlled custom-built adsorption cell (Harrick Scientific) were set in a dry nitrogen-purged chamber within the FTIR instrument.

**Fluorescence Recovery after Photobleaching.** The effect of ionic strength on the diffusion coefficient of PMAA* within PDMA/PMAA and Q100M/PMAA multilayer films was followed by FRAP

following a procedure similar to that reported by Jourdainne et al.[46] PDMA/PMAA and Q100M/PMAA multilayer films were prepared by LbL assembly within the homemade glass cells which were also used in the FCS experiments. For deposition of a surface priming layer, BPEI solution at pH 9 was injected into the cells for 15 min, followed by rinsing with Milli-Q water. All PA and PC solutions were controlled at pH 5 and room temperature. Multilayer films were then fabricated by alternating addition of PA or PC solutions into the cell for 15 min, with the application of two 1-min 0.01 M phosphate buffer rinsing cycles in between the polymer deposition steps. The film deposition was terminated with a PMAA layer. For deposition at pH 4.5−5.5, PMAA* was deposited within the third, fourth and fifth bilayers within the multilayer 'bulk', forming PEMs abbreviated as BPEI/PMAA/$(PC/PMAA)_2$/$(PC/PMAA^*)_3$/$(PC/PMAA)_2$. At pH 6−6.5, when the film grew exponentially, with a large amount of deposited polymer, including PMAA* deposited at each deposition step, it was sufficient to include only one rather than three marker layers to form the following PEM film: BPEI/PMAA/$(PC/PMAA)_2$/$(PC/PMAA^*)$/$(PC/PMAA)_2$. A circular region with a defined radius of 0.205 $\mu$m in the films was bleached for 10 s with a focused laser at 1 mW. Right after the bleaching procedure, the fluorescence intensity in the bleached zone was probed by a greatly attenuated beam (1 $\mu$W) to determine the bleaching efficiency, and then fluorescent intensity was recorded every 2−60 min (depending on the observed recovery kinetics) at 1 $\mu$W. Since the time required for recovery of fluorescence intensity in all experiments was much longer than the bleaching time (≥2 h vs 1 min), a contribution of molecular mobility during bleaching to the intensity recovery profile was considered negligible. All FRAP measurements were performed at 25 °C in 0.01 M phosphate buffer solutions at the same pH values which were used in deposition of PEMs.

## RESULTS AND DISCUSSION

Our main goal was to establish correlations between molecular mobility of PE chains when these chains were bound within polyelectrolyte complexes (PECs) or included within PEMs, and growth modes of LbL films. Results of measurements of molecular dynamics in solution were obtained using FCS and are presented in section I. Studies of PEM internal structure, dynamics of assembled chains, and measurements of ionization of PEs within LbL assemblies performed using NR, FRAP and ATR-FTIR techniques, respectively, are given in section II.

**I. Diffusion of PE Chains in Solution.** Studies of interactions between polyelectrolyte chains in solutions date back as far as the 1920s.[47] It was early realized that binding of oppositely charged chains in solution, often observed by turbidity as the formation of a liquid-like polymer-rich phase (or complex coacervation), or by complex precipitation, is dependent on a number of parameters, such as the type of interacting polyelectrolytes, the ratio of chain lengths, polyelectrolyte concentrations, PE mixing ratio, as well as the ionic strength and pH of the solution. Significant experimental and theoretical efforts have been made to develop a better understanding of those dependences for both strong and weak polyelectrolyte pairs.[30,31,33] Here, inspired by other earlier studies of the dynamics of interacting polyelectrolyte chains in solution using the fluorescence quenching technique,[48] we aim to contribute to a molecular-level understanding of the formation of PECs in solution. We achieve this by applying FCS—a technique capable of monitoring diffusion and the hydrodynamic sizes of individually dispersed PEC particles in solution. Furthermore, we aim to directly relate the FCS results with trends in PEM formation.

*Diffusion of Individual PE Chains in Solution as a Function of pH.* Figure 1 shows typical spectra of normalized autocorrelation functions (ACFs) of molecular mobility in

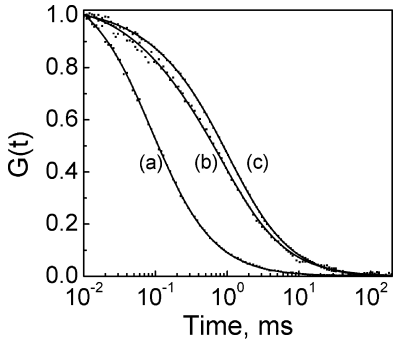


**Figure 1.** Normalized autocorrelation data for diffusion of free Alexa Fluor 488 hydrazide in 2 nM solution at pH 9 (a) and PMAA* chains with a concentration of $10^{-4}$ mg/mL in 0.01 M phosphate buffer solution at pH 4.5 and 6 (b and c), respectively. Data were fitted with eq 2. $D$ of free Alexa 488 hydrazide was ~430 $\mu m^2/s$ and $D$s of PMAA* were ~45 $\mu m^2/s$ and ~35 $\mu m^2/s$ at pH 4.5 and 6, respectively.

aqueous solution. During fitting, the points at time ranges shorter than 5 $\mu$s were discarded due to detector after-pulsing.[49] As shown in Figure 1, ACFs were successfully fitted using eq 2 with a single diffusion time mode for both the free Alexa 488 hydrazide label, and solutions of PMAA*. These results confirm that PMAA* solutions did not contain traces of unattached free Alexa 488 label. The fitting procedure gave a value of $D$ for free Alexa 488 hydrazide of ~430 $\mu m^2/s$, which is consistent with the literature.[50] Importantly, ACFs for PMAA* solutions had distinctly lower $D$s which were also dependent on solution pH (~45 $\mu m^2/s$ at pH 4.5 and ~35 $\mu m^2/s$ at pH 6, respectively), as expected for a weak polyacid. Figure 2

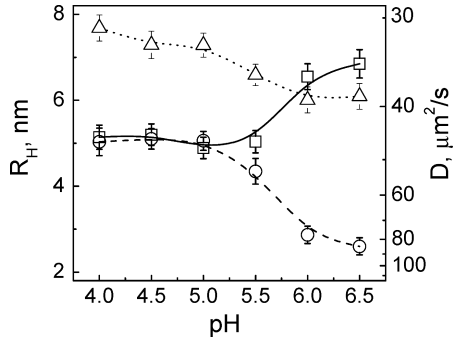


**Figure 2.** The pH dependences of the diffusion coefficients $D$ and hydrodynamic radii $R_H$ in 1 × $10^{-4}$ mg/mL PMAA* (squares), PDMA* (circles), and Q100M* (triangles) solutions obtained by FCS. The solution pH was supported by 0.01 M phosphate buffer. All solutions were controlled at 25 °C.

summarizes the pH dependences of the diffusion coefficients and hydrodynamic radii with 1 × $10^{-4}$ mg/mL PDMA*, Q100M*, and PMAA* in 0.01 M phosphate buffer solutions. Figure S2 in the Supporting Information shows results of control experiments, in which freely diffusing, unattached Alexa 488 dye was mixed with unlabeled PMAA, PDMA, or Q100 M in the same ratio as in Figure 2. The diffusion coefficient of free Alexa 488 was constant and unaffected by the presence of unlabeled polymers within the entire pH range of 4−7, suggesting the absence of noncovalent interactions between free Alexa 488 dye and polyelectrolyte chains. Unlike with hydrophobic dyes, the labeling of the hydrophilic Alexa 488 dye


dx.doi.org/10.1021/ma300157p | Macromolecules 2012, 45, 3892−3901

has no significant effect on the conformation and diffusion of polymer chains.[51]

Each point in Figure 2 was obtained by averaging three measurement results, and error bars represent the standard deviation of those measurements. At the very low concentration of $1 \times 10^{-4}$ mg/mL (~2 chains/$\mu m^3$) used in these experiments, the average number of polymer chains in the excitation volume was less than one. Since the average chain-to-chain distance was over 2 orders of magnitude larger than the hydrodynamic radii of the coils (2−8 nm, as will be shown below) and the Debye length of the solution (<3 nm), polymer chains can be considered as isolated noninteracting coils. The hydrodynamic radius $R_H$ of diffusing polymer coils was calculated from $D$ based on the Stokes−Einstein equation. The absolute values of $R_H$ also indicate that polymer chains exist as individual polymer coils rather than chain aggregates. As shown in Figure 2, increasing solution pH results in an increase of diffusion coefficient for PDMA* and a decrease of diffusion coefficient $D$ for PMAA*. This pH dependence reflects PE chain expansion/contraction caused by changes in PE ionization, and is in good agreement with earlier reported p$K_a$ values of PMAA at 6.5 and PDMA at 6.7.[74] An estimate of the persistence length, $l_p$, of neutral PMAA chains at pH 4 following a random-coil model gave a value 4.8 Å, which agrees well with small-angle X-ray scattering(SAXS) measurements.[52] The hydrodynamic radius $R_H$ of PMAA doubles between pH values of 4 and 6.5 as PMAA becomes more ionized, again in agreement with the pH dependence of the radii of gyration $R_G$ of PMAA chains measured via small-angle neutron scattering (SANS),[53,54] as well as our earlier FCS data.

It is interesting to compare the data for PDMA and Q100M polycations, as these PCs were obtained from the same parent polymer, and differ only in their side group bulkiness and pH response. First, complete quaternization of DMA units in Q100M chains significantly suppresses the pH dependence of $R_H$, as expected. The residual slight pH dependence is probably due to the additional salt ions added to solutions at higher pH during titration of the phosphate buffer, as well as due to possible differences in hydration of Q100M at low and neutral pH values. Most interestingly, at low pH values, when both PCs are fully charged, the $R_H$ of Q100M is ~1.5-fold larger than that of PDMA. This suggests that quaternization of the tertiary amino group of PDMA to produce Q100M with three methyl groups at the nitrogen atom enhances steric hindrance to rotation, increasing chain rigidity. These results show that facile, quick, in-house measurements of the $R_H$ of isolated PE chains using FCS can provide a wealth of information about the conformational changes of isolated polyelectrolyte chains in solution as a function of multiple experimental parameters.

*Diffusion of Water-Soluble PECs in Solution as a Function of pH.* Prior studies showed that with many types of PEs, water-soluble PECs (WPECs) are formed in asymmetric mixtures of oppositely charged PEs, i.e. when the ratio of total positive-to-negative charge on the polymers in the system is much smaller or much larger than unity.[55,56] These studies mostly involved highly hydrated carboxylate or phosphate polyanions and tertiary or quaternary ammonium polybases. For these easily equilibrated WPEC systems consisting of polyamines with tertiary or quaternary amino groups and polyacids with carboxylate or phosphate groups, it was shown that WPECs are thermodynamically stable structures, with a measurable chain transfer rate between molecularly dispersed complexes.[57]

The polycations studied here—PDMA and Q100M—represent secondary and tertiary polyamines. Since these PEs have identical chain lengths and molecular polydispersity, it is interesting to compare their behavior during binding with the same PA in identical experimental conditions. Note that such studies have not yet been reported. The application of FCS is most appropriate for these studies, as the technique enables observing not only the average hydrodynamic sizes of diffusing WPECs, but also their size distributions, indicative of equilibration of PEs between WPEC diffusing particles.

In all experiments, a 10-fold excess of PC (PDMA and Q100M) was added to a $10^{-4}$ mg/mL PMAA* solution. In both cases, mixtures of the two oppositely charged polyelectrolytes remained transparent. This result is consistent with an earlier report by Spruijt et al. that PDMA and a poly(carboxylic acid) form water-soluble complexes in extremely dilute solutions.[32] The diffusion coefficients and hydrodynamic sizes of the WPEC particles of PC/PMAA* were monitored by FCS. Figure S3 in the Supporting Information shows the kinetics of formation of PDMA/PMAA* and Q100M/PMAA* PECs (w:w = 10:1) in solution. The size of the complexes reaches a steady state ~10 min after mixing. The average $D$s and size distributions of the complexes remain constant after this initial equilibration time, even after as long as 24 h (data not shown). Figure 3 shows the average $R_H$ and the size distribution of PECs

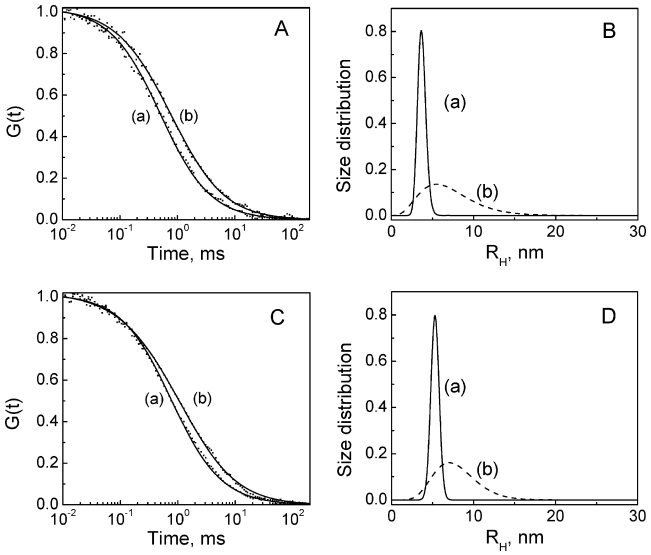


**Figure 3.** ACF (left panels) and size distributions (right panels) of (A and B) PDMA/PMAA* and (C and D) Q100M/PMAA* complexes at pH 6 (a, solid lines) and 4.5 (b, dashed lines), respectively.

at lower pH and higher pH values for both PE pairs. Right panels in Figure 3 show distributions of $R_H$ obtained from analysis of FCS data suggesting a log-normal WPEC size distribution. Similar data obtained in the range of pH from 4 to 6.5 for PDMA/PMAA* and Q100M/PMAA* PECs in solution after 30 min of mixing are shown in Figure 4. The hydrodynamic radii $R_H$ of PEC particles, specifically in the case of PDMA/PMAA*, decrease with increasing solution pH. This pH dependence suggests that WPECs are enriched with PCs, which were added in 10-fold excess to the solution mixture. The observation of the fluorescent intensity of PECs, of course, proves the presence of PMAA* within PECs. Since the zero time correlation $G(0)$ is inversely proportional to the average number of molecules in the excitation volume, analysis


dx.doi.org/10.1021/ma300157p | Macromolecules 2012, 45, 3892−3901

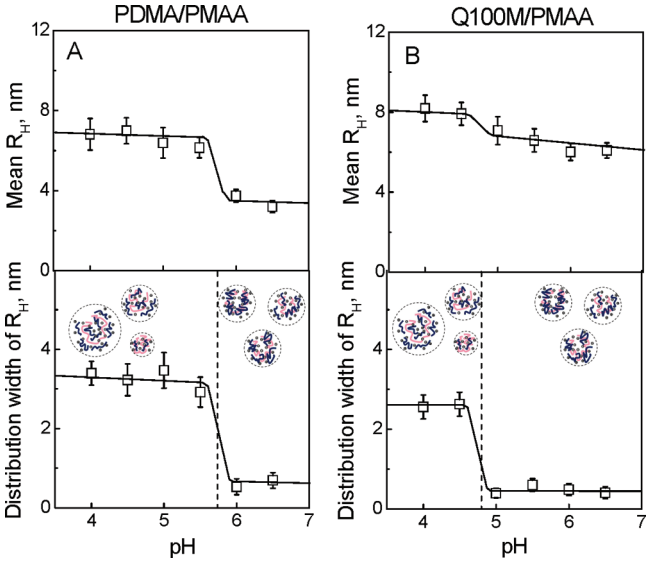


**Figure 4.** pH dependence of mean values (top panels) and distribution widths (bottom panels) of hydrodynamic radii $R_H$ of PDMA/PMAA* (A) and Q100M/PMAA* (B) PECs, respectively, measured by FCS. The distribution width is estimated as the standard deviation of the suggested log-normal $R_H$ distribution. Squares are average values of three independent measurements and error bars are one standard deviation. The concentration of PMAA* is $1 \times 10^{-4}$ mg/mL in 0.01 M phosphate buffer, and the mass ratio of PCs and PMAA* is 10:1. Solid lines are just eye guides.

of $G(0)$ of the PMAA* solution before and after addition of PDMA showed that WPECs contained on average one PMAA* chain (data not shown).[58,59] The hydrodynamic size of WPECs in Figures 3 and 4 differs from that of the initial PEs in Figure 2, yet is within a similar size range, in agreement with the absence of aggregation of WPEC particles. Considering the similar degrees of polymerization of PCs and PAs, one also concludes that there is more than one molecule of PC within WPECs attached to a PMAA* chain. Earlier, similar nonstoichiometric complexes enriched and solubilized by PCs were reported in a different system.[60] No data on hydrodynamic sizes and their distribution could be obtained in those earlier studies because of limitations of traditional steady-state fluorometry measurements. However, a model for nonstoichiometric complexes has been suggested, that assumes that the PEC particles consist of a stoichiometric, charge compensated and more hydrophobic core, and a more hydrophilic, positively charged outer shell formed by excess PC chains.[33,61]

Probably the most striking observation in Figures 3 and 4 is that, for both types of WPECs, the distribution of $R_H$ is drastically different at various pH values. The WPEC size exhibited a wide dispersion at lower pH values, and showed a narrower dispersion at higher pHs. A wide distribution of $R_H$ at lower pH values indicates a broad range of compositions of coexisting WPECs, and suggests kinetically trapped, non-equilibrated states. In an earlier work, we suggested that protonated carboxylic groups can "pin" macromolecules within PE multilayers in acidic media through formation of hydrogen bonded dimers,[62,63] but this explanation is unlikely to apply to the ultradilute solutions of PECs shown in Figure 4. While it is clear that sluggish exchange in PECs correlates with a low degree of polyacid ionization, the exact origin of this phenomenon remains unclear. An intriguing possibility that changes in the hydration state of poly(carboxylic acid)s affect the binding strength of oppositely charged polyelectrolytes[64−66] and therefore the dynamics of PECs, is worth exploring in the future. At high pH values, the ionization of PMAA* increases, and the $R_H$ distribution of PECs becomes drastically more narrow, due to facilitated chain exchange and equilibration of WPEC conformations. Earlier studies of equilibrated states of WPECs in this regime revealed several intriguing phenomena of selective binding of PEs within WPECs based on their chain length,[45,67] charge density,[68,69] PE type,[70] and even the type of small ions present in solution.[71]

This result also provides a hint as to the role of PE type on the dynamics of PE chain exchange between PEC particles. For example, in the entire pH range, the distribution widths of $R_H$ in the Q100M/PMAA system were lower than those in PDMA/PMAA mixtures (Figure 4, lower panels), possibly suggesting better chain equilibration in the system containing the completely quaternized polycation. In addition, the pH range at which the transition between the nonequilibrated and equilibrated regimes occurs differed for the two PE systems (Figure 4). The transition occurs between pH 5.5 and 6 for PDMA/PMAA* PECs, and at a lower pH range from 4.5 to 5 for Q100M/PMAA*. These transition intervals are termed $\Delta pH_{tr}$. Prior to discussing possible origins of these differences, we sought to find out whether the transition pH intervals found

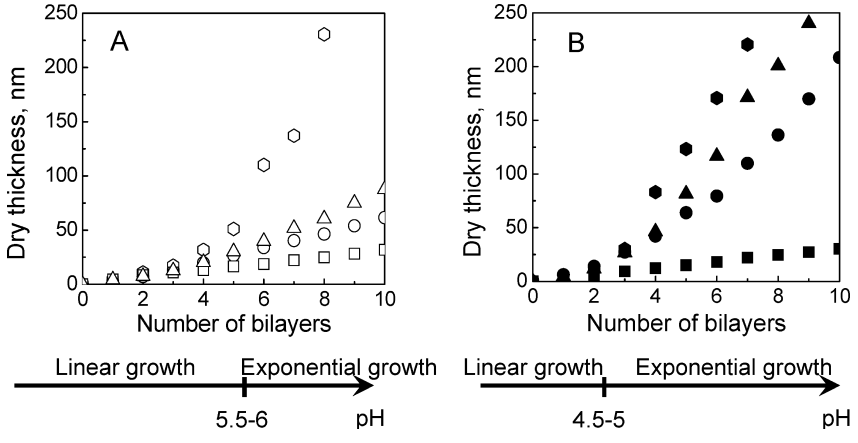


**Figure 5.** Dry film thicknesses of (A) PDMA/PMAA and (B) Q100M/PMAA PEMs deposited at pH 4.5 (squares), 5 (circles), 5.5 (triangles), and 6 (hexagons) as followed by ellipsometry.


dx.doi.org/10.1021/ma300157p | *Macromolecules* 2012, 45, 3892−3901

for PECs would also be indicative of significant changes in the structure of PEM films.

**II. Film Structure and Chain Dynamics in PEMs.**

*II. Deposition of PEMs at Various pH Values and Ionization of a Polyacid within PEM Films.* Figure 5 shows dry thicknesses of PDMA/PMAA and Q100M/PMAA during PEM film deposition on a silicon wafer as monitored by phase-modulated ellipsometry. Clearly, the growth profile of PEMs is dependent on the pH of the deposition solutions. The film thickness increased in a linear manner at lower deposition pH, and exhibited an exponential growth profile at higher pHs. The transition between the two growth regimes occurred exactly within the same pH interval $\Delta pH_{tr}$ (pH 5.5−6 for PDMA/PMAA*, and pH 4.5−5 for Q100M/PMAA*) in which the transition between kinetically trapped and equilibrated PECs was observed in solution (Figure 4). This result establishes a direct correlation between the dynamics of PE chains within PECs and the mode of growth of PEM films. It is obvious from a comparison of Figures 4 and 5 that fast exchange of PEs in PECs and equilibrated, narrow-size-distribution WPECs are related to an exponential deposition of PEM films. At the same time, strong and irreversible binding of polymer chains within PECs is predictive of linear deposition of multilayer films. Therefore, rapid FCS-based assessment of the dynamics of PECs in solution can be used as a convenient tool to predict deposition modes of polymer chains at surfaces.

Seeking to understand the origin of the difference in the $\Delta pH_{tr}$ values for the PDMA/PMAA* and Q100M/PMAA* systems (observed both for PECs and PEMs), we first hypothesized that this effect is due to differences in charge density in PDMA and Q100M in the neutral pH range. PCs with higher charge density have been demonstrated to induce stronger ionization of poly(carboxylic acid)s.[45] This line of argument also presumes that $\Delta pH_{tr}$ values are exclusively determined by the ionization degree of PMAA, and that the transition occurs at a universally critical degree of polyacid ionization.[62,63] To check the validity of this hypothesis in the case of PDMA/PMAA and Q100M/PMAA multilayers, we applied *in situ* ATR-FTIR in order to quantify the ionization degrees of PMAA within PDMA/PMAA and Q100M/PMAA films. Figure S4 in the Supporting Information shows that infrared spectra of these multilayers assembled and probed in $D_2O$ solutions at pH 5 exhibited two major peaks: an absorption band at 1702 $cm^{-1}$ associated with stretching vibrations of the uncharged carboxylic acid group ($\nu_1$, C═O), and a band at 1552 $cm^{-1}$ assigned to asymmetric stretching vibrations of the carboxylate group ($\nu_2$, $COO^-$).[72] Earlier reports showed that the extinction coefficients of these two bands are equal.[73,74] Hence, the degree of ionization of PMAA can be obtained from the ratio of the band area at 1552 $cm^{-1}$ to the sum of peak areas at 1552 and 1702 $cm^{-1}$. Peak areas were determined from a curve-fitting procedure using Origin 8.0 software under the assumption of a Gaussian shape. The degrees of ionization of PMAA within $(PDMA/PMAA)_5$ and $(Q100M/PMAA)_5$ PEMs were thus obtained as ∼70% and ∼55%, respectively. In other words, the higher-charge-density Q100M induces lower ionization of its PMAA partner. This result suggests that ionization of a weak polyacid is not the only factor determining the boundaries between frozen and equilibrated PECs and linearly and exponentially growing PEMs on the pH scale.

Moreover, the result also suggests that regardless of the charge density of the assembled polycations, a PC with more steric bulk at the ionic group (i.e., Q100M) was less efficient at inducing ionization of assembled PMAA, due to an increased distance between the positive charge at the nitrogen atom in Q100M chains and the carboxylic acid group in PMAA. These data are consistent with reports from other groups on the dependence of ionization of a weak polyacid on polycation type assembled within PEMs. These earlier results were explained by the influence of the hydrophobicity of polycations rather than by the steric bulk at the charged group.[75,76] The consequence of steric hindrance at the cationic group is a weaker electrostatic bonding energy between oppositely charged layers in Q100M/PMAA PEMs. In our previous work, steric hindrance was found to be an important factor determining the internal structure and mobility of polyelectrolyte chains.[34] PEs with higher steric hindrance to ionic pairing were more prone to chain intermixing within PEMs during annealing in salt solutions.[28,34] Here, we show that the steric influence on ionic pairing affects both mutual ionization of assembled weak PEs and growth of multilayer films. Later in this chapter, we will also explore the effects of the strength of ionic paring on lateral mobility of PE chains within PEM films.

After exploring possible reasons for pH-governed linear-to-exponential growth transitions in PEMs, we turned to analysis of internal film structure in various pH regions.

*Film Structure as Studied by Neutron Reflectometry.* Figure 6 shows neutron reflectivity data of 20-bilayer PDMA/PMAA and Q100M/PMAA films (panels A and B, respectively) deposited at a series of pHs. To provide NR contrast, deuterated PMAA, dPMAA, was deposited within each fifth bilayer of the film. The data are presented as neutron reflectivity $R$ plotted as a function of momentum transfer $Q$. The scattering densities, layer thicknesses and internal roughnesses within the multilayer films in Figure 5 are summarized in Table S1 in the Supporting Information. The dry thicknesses of films determined from NR data were ∼20% smaller than those obtained by ellipsometry, possibly because of differences in ambient air humidity during the respective measurements.[77] NR data were fitted by diffuse layers which indicated significant layer intermixing. However, a set of well-developed Bragg peaks and Kiessig fringes are obvious in the data for PDMA/PMAA films deposited at pH 4.5 and 5.5, as well as for Q100M/PMAA films deposited at pH 4.5. For these films, the thickness of dPMAA marker layers increased with distance from the substrate as a result of intermixing with the neighboring hydrogenated matrix, and increased from 38 to 39

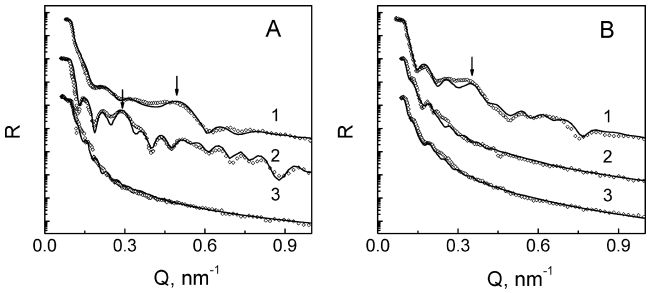


**Figure 6.** Plot of reflectivity $R$ vs $Q$ of dry $[(PC/PA)_4/(PC/dPA)]_4$ films for (A) PDMA/PMAA and (B) Q100M/PMAA with dPMAA in each fifth bilayer deposited at pH 4.5, 5.5, and 6 (top to bottom), respectively. Arrows indicate the 1st superlattice peaks, which move to lower $Q$ values with increasing pH, indicating deposition of thicker layers (bilayer thickness ∼1/$Q$).

Å for the closest-to-the substrate marker layer to 60−67 Å for the layer closest to the air interface (see Table S1 in the Supporting Information). Within the ∼15% accuracy of the fitting procedure, this trend was similar for all films mentioned above. The presence of film stratification is consistent with the ellipsometrically determined linear growth of films in these conditions (Figure 5). Also in agreement with ellipsometric results, parts A and B of Figure 6 illustrate the lack of Bragg peaks in the NR curves for PDMA/PMAA films deposited at pH 6 and for Q100M/PMAA films deposited at pH 5.5 and 6, suggesting complete layer intermixing resulting from high mobility of PE chains during PEM deposition, as is usually observed with the exponential growth of PEM films.[44,78,79] Taken together, NR results are consistent with FCS and ellipsometry data, and provide direct evidence of lamellar structure in linearly deposited films, and complete chain intermixing in exponentially deposited multilayers.

*Chain Dynamics Studied by FRAP.* Finally, it was interesting to perform a comparative study of the lateral mobility of PEs within PEMs in the linear and exponential growth regimes for PDMA and Q100M PCs differing in their pH dependence of charge density, as well as in steric bulk at ionic groups. While previous studies reported lateral diffusion coefficients of PEM films of different compositions deposited either linearly or exponentially, here we make a side-by-side comparison of the lateral mobility of PEs within PEMs of the same composition deposited either linearly or exponentially depending on the solution pH. To that end, we constructed PEMs containing PMAA*, and performed spot-bleaching FRAP experiments. After bleaching of film fluorescence at high laser power, fluorescence recovery at the bleached spot was recorded at much lower laser intensity as a function of time. Assuming the diffusion of polymer chains both perpendicular and parallel to the substrate follows a Gaussian distribution of the chain displacement probability, the lateral diffusion coefficient ($D_{||}$) of PMAA* within PEMs was calculated as[80] $D_{||} = \gamma R^2/4t_{1/2}$ (where shape factor $\gamma$ is 0.88 for a spherical beam spot, and $R$ = 0.205 $\mu$m is the radius of the bleaching spot, determined from measurements of the diffusion of free Rhodamine-110). Multilayers were deposited on the cover glass of a glass cell primed with a monolayer of BPEI, as described in the Experimental Section. To establish the appropriate polymer deposition sequence for such studies, we constructed a series of PMAA*-containing PEMs with different positions of a PMAA* marker layer within the film. This series included 5 PEM films, starting from one containing PMAA* as the top layer BPEI/PMAA/$(PDMA/PMAA)_4$/(PDMA/PMAA*) (see Figure S5 in the Supporting Information) and ending with a BPEI/PMAA/(PDMA/PMAA*)/$(PDMA/PMAA)_4$ film. Experiments with these films revealed that (a) PMAA* included within the two bilayers closest to the substrate/water interface was about half/twice as mobile as the PMAA* included within the central film layers, respectively (in agreement with previous reports[28,81]) and that (b) PMAA* marker layers deposited in the central region of exponentially growing PEMs showed consistent mobility (within ∼10%, data not shown). All experiments shown below were performed with multilayers featuring the following deposition sequence: BPEI/PMAA/$(PDMA/PMAA)_2$/(PDMA/PMAA*)/$(PDMA/PMAA)_2$, in which PMAA* was included within the central region of the film.

Regardless of the deposition pH, none of the multilayers showed significant mobility of PMAA* marker layers in FRAP experiments within a measurement time of 2−3 days unless PEMs were exposed to solutions with high concentrations of sodium chloride. The latter promoted ion doping and facilitated molecular mobility within the films. For PDMA/PMAA and Q100M/PMAA multilayers, raising salt concentration to 0.2 M NaCl was sufficient to induce experimentally measurable diffusion of PMAA* chains.[28] Here, we controlled the salt concentration of annealing solutions shown above at 0.4 M NaCl. The effects of pH in high-salt solutions on the lateral diffusion coefficient of PMAA* within the PDMA/PMAA and Q100M/PMAA PEMs are shown in Figure 7. First,

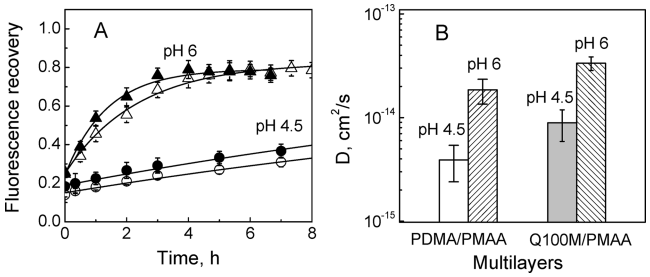


**Figure 7.** (A) Recovery of fluorescence intensity and (B) calculated diffusion $D_{||}$ of PMAA* coefficients in FRAP experiments with $(PC/PMAA)_2/(PC/PMAA^*)_3/(PC/PMAA)_2$ multilayers exposed to 0.4 M NaCl solutions at pH 4.5 (circles) and pH 6 (triangles). PDMA/PMAA, open symbols; Q100M/PMAA films, filled symbols.

a clear difference is observed for both PEM systems between a lower pH regime of linearly growing films, and a higher pH region of exponentially growing PEMs. For both polymer systems, the diffusion coefficient in the direction parallel to the surface ($D_{||}$) of PMAA* measured by FRAP differed about 5-fold between pH 4.5 and pH 6 (linear and exponential growth regimes, respectively). For example, $D_{||}$ of PMAA* increased from $(4 \pm 1.5) \times 10^{-15}$ to $(1.8 \pm 0.7) \times 10^{-14}$ cm$^2$/s between the linear and exponential growth regimes for PDMA/PMAA films. Importantly, following our earlier suggestion regarding the significant role of steric bulk on chain mobility within PECs and PEMs (Figures 4 and 5), application of FRAP provided direct experimental evidence of this effect. As Figure 7 illustrates, the values of $D_{||}$ of PMAA* within Q100M/PMAA multilayers at corresponding pH values [$(8 \pm 3) \times 10^{-15}$ cm$^2$/s at pH 4.5 and $(3.4 \pm 1.2) \times 10^{-14}$ cm$^2$/s at pH 6] were about twice as large as those for PDMA/PMAA films. This result demonstrates that steric bulk (i.e., the extra methyl group) introduced by quaternization is an essential factor determining PE chain mobility. This conclusion is applicable to both linear and exponential growth regimes of PEM films. Weaker electrostatic ionic pairing between Q100M and PMAA compared to that between PDMA and PMAA is also consistent with ATR-FTIR data above on PC-induced ionization of PMAA within PEM films.

## ■ CONCLUSIONS

Using polycations with different steric bulk at the ionic group, we have established a correlation between the dynamics of polyelectrolyte chains in PC/PMAA PECs, and the deposition mode (linear versus exponential) of PEM films. The behavior of PEMs "mirrored" the solution behavior of PC/PMAA mixtures, showing a transition from linear to exponential film growth regimes exactly at the same pH values where switching between nonequilibrated and equilibrated PECs occurred. NR experiments with PEMs containing deuterated PMAA as

marker layers confirmed a transition between the deposition of stratified and completely intermixed films as a function of pH. The specific value of transition pH between the two modes of PEM deposition was dependent on polyelectrolyte type, and specifically on the ionization degree and steric bulk at the ionic group of PCs. FRAP experiments performed on linearly and exponentially grown films confirmed the higher mobility of PMAA* within assemblies when the polyacid is bound with Q100M (rather than with PDMA) due to greater steric restriction to ionic pairing. In addition, within both Q100M/PMAA and PDMA/PMAA multilayer films, the diffusion coefficient of assembled PMAA* in the exponential regime was ∼5-fold higher than that in the linear regime. These results further contribute to understanding the relationships between ionization, PE type and molecular structure of polyelectrolyte and chain dynamics within LbL films.

## ■ ASSOCIATED CONTENT

### Supporting Information

The fitting parameters of neutron reflectivity, $^1$H NMR spectra, pH dependence of diffusion coefficients and hydrodynamic radii, kinetics of formation, comparison of ATR-FTIR spectra, and time recovery of fluorescence intensity. This material is available free of charge via the Internet at http://pubs.acs.org.

## ■ AUTHOR INFORMATION

### Corresponding Author

*E-mail: ssukhish@stevens.edu.

### Notes

The authors declare no competing financial interest.

## ■ ACKNOWLEDGMENTS

We thank Thomas Cattabiani (Stevens Institute of Technology) for his useful discussions. This work was supported by the National Science Foundation under Award DMR-0906474. The neutron reflectometry measurements were performed at the Spallation Neutron Source at the Oak Ridge National Laboratory, managed by UT-Battelle, LLC, for the DOE under Contract No. DE-AC05-00OR22725.

## ■ REFERENCES

(1) Decher, G. *Science* **1997**, *277*, 1232.
(2) Bédard, M. F.; De Geest, B. G.; Skirtach, A. G.; Möhwald, H.; Sukhorukov, G. B. *Adv. Colloid Interface Sci.* **2010**, *158*, 2.
(3) Pavlukhina, S.; Sukhishvili, S. A. *Adv. Drug Delivery Rev.* **2011**, *63*, 822.
(4) Zhu, Z. C.; Sukhishvili, S. A. *ACS Nano* **2009**, *3*, 3595.
(5) Kharlampieva, E.; Ankner, J. F.; Rubinstein, M.; Sukhishvili, S. A. *Phys. Rev. Lett.* **2008**, *100*, 128303.
(6) Kharlampieva, E.; Kozlovskaya, V.; Sukhishvili, S. A. *Adv. Mater.* **2009**, *21*, 3053.
(7) Elbert, D. L.; Herbert, C. B.; Hubbell, J. A. *Langmuir* **1999**, *15*, 5355.
(8) Picart, C.; Lavalle, P.; Hubert, P.; Cuisinier, F. J. G.; Decher, G.; Schaaf, P.; Voegel, J.-C. *Langmuir* **2001**, *17*, 7414.
(9) Halthur, T. J.; Elofsson, U. M. *Langmuir* **2004**, *20*, 1739.
(10) Richert, L.; Lavalle, P.; Payan, E.; Shu, X. Z.; Prestwich, G. D.; Stoltz, J. F.; Schaaf, P.; Voegel, J. C.; Picart, C. *Langmuir* **2004**, *20*, 448.
(11) Picart, C.; Mutterer, J.; Richert, L.; Luo, Y.; Prestwich, G. D.; Schaaf, P.; Voegel, J.-C.; Lavalle, P. *Proc. Natl. Acad. Sci. U.S.A.* **2002**, *99*, 12531.
(12) Lavalle, P.; Picart, C.; Mutterer, J.; Gergely, C.; Reiss, H.; Voegel, J.-C.; Senger, B.; Schaaf, P. *J. Phys. Chem. B* **2004**, *108*, 635.
(13) Yoo, P. J.; Nam, K. T.; Qi, J.; Lee, S.-K.; Park, J.; Belcher, A. M.; Hammond, P. T. *Nat. Mater.* **2006**, *5*, 234.
(14) Fu, J. H.; Ji, J.; Shen, L. Y.; Kueller, A.; Rosenhahn, A.; Shen, J. C.; Grunze, M. *Langmuir* **2009**, *25*, 672.
(15) Lavalle, P.; Voegel, J.-C.; Vautier, D.; Senger, B.; Schaaf, P.; Ball, V. *Adv. Mater.* **2011**, *23*, 1191.
(16) Porcel, C.; Lavalle, P.; Decher, G.; Senger, B.; Voegel, K. C.; Schaaf, P. *Langmuir* **2007**, *23*, 1898.
(17) Hoda, N.; Larson, R. G. *J. Phys. Chem. B* **2009**, *113*, 4232.
(18) Laugel, N.; Betscha, C.; Winterhalter, M.; Voegel, J.-C.; Schaaf, P.; Ball, V. *J. Phys. Chem. B* **2006**, *110*, 19443.
(19) Tan, W. S.; Cohen, R. E.; Rubner, M. F.; Sukhishvili, S. A. *Macromolecules* **2010**, *43*, 1950.
(20) Liu, G. M.; Zhao, J. P.; Sun, Q. Y.; Zhang, G. Z. *J. Phys. Chem. B* **2008**, *112*, 3333.
(21) Salomaki, M.; Laiho, T.; Kankare, J. *Macromolecules* **2004**, *37*, 9585.
(22) Dubas, S. T.; Schlenoff, J. B. *Macromolecules* **1999**, *32*, 8153.
(23) Salomäki, M.; Vinokurov, I. A.; Kankare, J. *Langmuir* **2005**, *21*, 11232.
(24) Sun, B.; Jewell, C. M.; Fredin, N. J.; Lynn, D. M. *Langmuir* **2007**, *23*, 8452.
(25) Itano, K.; Choi, J.; Rubner, M. F. *Macromolecules* **2005**, *38*, 3450.
(26) Mauser, T.; Déjugnat, C.; Möhwald, H.; Sukhorukov, G. B. *Langmuir* **2006**, *22*, 5888.
(27) Gucht, J. V. D.; Spruijt, E.; Lemmers, M.; Cohen Stuart, M. A. *J. Colloid Interface Sci.* **2011**, *361*, 407.
(28) Xu, L.; Kharlampieva, E.; Izumrudov, V.; Ankner, J. F.; Sukhishvili, S. A. *ACS Macro Lett.* **2012**, *1*, 127.
(29) Mjahed, H.; Voegel, J.-C.; Chassepot, A.; Senger, B.; Schaaf, P.; Boulmedais, F.; Ball, V. *J. Colloid Interface Sci.* **2010**, *346*, 163.
(30) Biesheuvel, P. M.; Cohen Stuart, M. A. *Langmuir* **2004**, *20*, 2785.
(31) Biesheuvel, P. M.; Cohen Stuart, M. A. *Langmuir* **2004**, *20*, 4764.
(32) Spruijt, E.; Westphal, A. H.; Borst, J. W.; Cohen Stuart, M. A.; van der Gucht, J. *Macromolecules* **2010**, *43*, 6476.
(33) Chollakup, R.; Smitthipong, W.; Eisenbach, C. D.; Tirrell, M. *Macromolecules* **2010**, *43*, 2518.
(34) Xu, L.; Ankner, J. F.; Sukhishvili, S. A. *Macromolecules* **2011**, *44*, 6518.
(35) Tan, S. L.; Erol, M.; Sukhishvili, S. A.; Du, H. *Langmuir* **2008**, *24*, 4765.
(36) Ydens, I.; Moins, S.; Degeé, P.; Dubois, P. *Eur. Polym. J.* **2005**, *41*, 1502.
(37) Petzhold, C. L.; Stefens, J.; Monteavaro, L. L.; Stadler, R. *Polym. Bull.* **2000**, *44*, 477.
(38) Pristinski, D.; Kozlovskaya, V.; Sukhishvili, S. A. *J. Chem. Phys.* **2005**, *122*, 014907.
(39) Funhoff, A. M.; van Nostrum, C. F.; Koning, G. A. *Biomacromolecules* **2004**, *5*, 32.
(40) Magde, D.; Elson, E.; Webb, W. W. *Phys. Rev. Lett.* **1972**, *29*, 705.
(41) Rigler, R.; Mets, U.; Widengren, J.; Kask, P. *Eur. Biophys. J. Biophys. Lett.* **1993**, *22*, 169.
(42) Sukhishvili, S. A.; Chen, Y.; Muller, J. D.; Gratton, E.; Schweizer, K. S.; Granick, S. *Macromolecules* **2002**, *35*, 1776.
(43) Argón, S. R.; Pecora, R. *J. Chem. Phys.* **1976**, *64*, 1791.
(44) Kharlampieva, E.; Kozlovskaya, V.; Ankner, J. F.; Sukhishvili, S. A. *Langmuir* **2008**, *24*, 11346.
(45) Kharlampieva, E.; Sukhishvili, S. A. *Langmuir* **2003**, *19*, 1235.
(46) Jourdainne, L.; Arntz, Y.; Senger, B.; Debry, C.; Voegel, J.-C.; Schaaf, P.; Lavalle, P. *Macromolecules* **2007**, *40*, 316.
(47) Bungenberg de Jong, H.; Kruyt, H. *Proc. Sect. Sci., K. Ned. Akad. Wetenschappen* **1929**, *32*, 849.
(48) Kabanov, V. A.; Zezin, A. B. *Pure Appl. Chem.* **1984**, *56*, 343.
(49) Krichevsky, O.; Bonnet, G. *Phys. Prog. Rep.* **2002**, *65*, 251.
(50) Petrášek, Z.; Schwille, P. *Biophys. J.* **2007**, *94*, 1437.

(51) Morawetz, H. *Macromolecules* **1996**, *29*, 2689.
(52) Muroga, Y.; Yoshida, T.; Kawaguchi, S. *Biophys. Chem.* **1999**, *81*, 45.
(53) Magde, D.; Elson, E.; Webb, W. W. *Biopolymers* **1974**, *13*, 29.
(54) Pleštil, J.; Ostanevich, Y. M.; Bezzabotonov, V. Y.; Hlavatá, D.; Labský, J. *Polymer* **1986**, *27*, 839.
(55) Kabanov, V. A. Basic properties of soluble interpolyelectrolyte complexes applied to bioengineering and cell transformations. In *Macromolecular Complexes in Chemistry and Biology*; Dubin, P. L., Bock, J., Davis, R. M., Schulz, D. N., Thies, C., Eds.; Springer-Verlag: Berlin, 1994; pp 151.
(56) Sui, Z. J.; Jaber, J. A.; Schlenoff, J. B. *Macromolecules* **2006**, *39*, 8145.
(57) Bakeev, K. N.; Izumrudov, V. A.; Kuchanov, S. I.; Zezin, A. B.; Kabanov, V. A. *Macromolecules* **1992**, *25*, 4249.
(58) Berland, K. M.; So, P. T. C.; Gratton, E. *Biophys. J.* **1995**, *68*, 694.
(59) Chen, Y.; Müller, J. D.; So, P. T. C.; Gratton, E. *Biophys. J.* **1999**, *77*, 553.
(60) Izumrudov, V. A. *Russ. Chem. Rev.* **2008**, *77*, 381.
(61) Schatz, C.; Domard, A.; Viton, C.; Pichot, C.; Delair, T. *Biomacromolecules* **2004**, *5*, 1882.
(62) Izumrudov, V.; Sukhishvili, S. A. *Langmuir* **2003**, *19*, 5188.
(63) Izumrudov, V. A.; Kharlampieva, E.; Sukhishvili, S. A. *Biomacromolecules* **2005**, *6*, 1782.
(64) Farhat, T.; Yassin, G.; Dubas, S. T.; Schlenoff, J. B. *Langmuir* **1999**, *15*, 6621.
(65) Jaber, J. A.; Schlenoff, J. B. *Langmuir* **2007**, *23*, 896.
(66) Schlenoff, J. B.; Rmaile, A. H.; Bucur, C. B. *J. Am. Chem. Soc.* **2008**, *130*, 13589.
(67) Izumrudov, V. A.; Nyrkova, T. Yu.; Zezin, A. B.; Kabanov, V. A. *Vysokomolek. Soyed.* **1987**, *B29*, 474.
(68) Trukhanova, E. S.; Izumrudov, V. A.; Litmanovich, A. A.; Zelikin, A. N. *Biomacromolecules* **2005**, *6*, 3198.
(69) Zelikin, A. N.; Trukhanova, E. S.; Putnam, D. A.; Izumrudov, V. A.; Litmanovich, A. A. *J. Am. Chem. Soc.* **2003**, *125*, 13693.
(70) Izumrudov, V. A.; Kargov, S. I.; Zhiryakova, M. V.; Zezin, A. B.; Kabanov, V. A. *Biopolymers* **1995**, *35*, 523.
(71) Izumrudov, V. A.; Bronich, T. K.; Saburova, O. S.; Zezin, A. B.; Kabanov, V. A. *Makromol. Chem., Rapid Commun.* **1988**, *9*, 7.
(72) Kharlampieva, E.; Sukhishvili, S. A. *Macromolecules* **2003**, *36*, 9950.
(73) Xie, A. F.; Granick, S. *Macromolecules* **2002**, *35*, 1805.
(74) Sukhishvili, S. A.; Granick, S. *Macromolecules* **2002**, *35*, 301.
(75) Rmaile, H. H.; Schlenoff, J. B. *Langmuir* **2002**, *18*, 8263.
(76) Choi, J.; Rubner, M. F. *Macromolecules* **2005**, *38*, 116.
(77) Schmidt, S.; Hellweg, T.; von Klitzing, R. *Langmuir* **2008**, *24*, 12595.
(78) Jomaa, H. W.; Schlenoff, J. B. *Macromolecules* **2005**, *38*, 8473.
(79) Kharlampieva, E.; Ankner, J. F.; Rubinstein, M.; Sukhishvili, S. A. *Phys. Rev. Lett.* **2008**, *100*, 128303.
(80) Yoo, P. J.; Zacharia, N. S.; Doh, J.; Nam, K. T.; Belcher, A. M.; Hammond, P. T. *ACS Nano* **2008**, *2*, 561.
(81) Nazaran, P.; Bosio, V.; Jaeger, W.; Anghel, D. F.; von Klitzing, R. *J. Phys. Chem. B* **2007**, *111*, 8572.